Yeast cytochrome c integrated with electronic elements: a nanoscopic and spectroscopic study down to single-molecule level

2007 J. Phys.: Condens. Matter 19 225009

(http://iopscience.iop.org/0953-8984/19/22/225009)

IOP PUBLISHING JOURNAL OF PHYSICS: CONDENSED MATTER

J. Phys.: Condens. Matter **19** (2007) 225009 (18pp) doi:10.1088/0953-8984/19/22/225009

Yeast cytochrome c integrated with electronic elements: a nanoscopic and spectroscopic study down to single-molecule level

I Delfino[1], B Bonanni[1,2], L Andolfi[1], C Baldacchini[1,2], A R Bizzarri[1] and S Cannistraro[1]

[1] Biophysics and Nanoscience Centre, CNISM, Facoltà di Scienze, Università della Tuscia, I-01100 Viterbo, Italy
[2] CNR-INFM, Italy

E-mail: cannistr@unitus.it

Received 10 January 2007
Published 14 May 2007
Online at stacks.iop.org/JPhysCM/19/225009

Abstract

Various aspects of redox protein integration with nano-electronic elements are addressed by a multi-technique investigation of different yeast cytochrome c (YCC)-based hybrid systems. Three different immobilization strategies on gold via organic linkers are explored, involving either covalent bonding or electrostatic interaction. Specifically, Au surfaces are chemically modified by self-assembled monolayers (SAMs) exposing thiol-reactive groups, or by acid-oxidized single-wall carbon nanotubes (SWNTs). Atomic force microscopy and scanning tunnelling microscopy are employed to characterize the morphology and the electronic properties of single YCC molecules adsorbed on the modified gold surfaces. In each hybrid system, the protein molecules are stably assembled, in a native configuration. A standing-up arrangement of YCC on SAMs is suggested, together with an enhancement of the molecular conduction, as compared to YCC directly assembled on gold. The electrostatic interaction with functionalized SWNTs allows several YCC adsorption geometries, with a preferential high-spin haem configuration, as outlined by Raman spectroscopy. Moreover, the conduction properties of YCC, explored in different YCC nanojunctions by conductive atomic force microscopy, indicate the effectiveness of electrical conduction through the molecule and its dependence on the electrode material. The joint employment of several techniques confirms the key role of a well-designed immobilization strategy, for optimizing biorecognition capabilities and electrical coupling with conductive substrates at the single-molecule level, as a starting point for advanced applications in nano-biotechnology.

(Some figures in this article are in colour only in the electronic version)

1. Introduction

The successful introduction of a variety of nano-biosensors in environmental research, medical diagnostics, drug discovery and terrorism defence applications [1–4] has greatly increased the efforts for coupling biomolecules with non-biotic elements. In fact, a nano-biosensor is a nanometre-sized sensing device consisting of a biological recognition element in intimate contact with a suitable transducer, which is able to convert a biological function into a measurable (electrical, optical, electrochemical, thermometric, piezoelectric or magnetic) signal [2]. Since biomaterials and transducers are foreign components with respect ones to the others, some key requirements have to be fulfilled in designing such hybrid systems. The functionality of the biological recognition element is required to be preserved and the physiological conditions favouring the recognition should be guaranteed. Furthermore, the communication between the biomaterials and the corresponding transducers has to be optimized in order to maximize the sensitivity and reliability of the device. Then, once the hybrid system has been designed and implemented, a reliable characterization of its properties is needed.

Hybrid devices employing metalloproteins as the bioactive interface for electrical transduction represent one of the most extensively investigated systems [5–9]. Redox metalloproteins have an inherent very efficient electron transfer (ET) capability, occurring over long distances and in a very fast, directional way. These proteins are, in general, part of ET chains, where the conduction through the biomolecules occurs at the level of a single electron and offers the possibility of gating the redox activity [10, 11]. Cytochromes are among the best studied metalloproteins, because of their biological functions. They carry electrons in the photosynthetic and respiratory processes [12], involving the iron ion embedded in the haem redox centre, which switches its oxidation state between $+2$ and $+3$ in biological functioning. In mitochondrion, cytochrome c (cyt c) transfers electrons between two inner membrane-bound proteins, cyt c reductase and cyt c oxidase, by docking at specific binding sites to these redox partners. This makes cyt c very suitable as biological recognition element and signal transducer in biosensors, as demonstrated by its application in various devices [13, 14]. These achievements have boosted the efforts for realization and characterization of nanosized cyt c-based hybrid systems, thus renewing the attention to cyt c single-molecule interaction with electrode surfaces and with its redox partners in physiological-like conditions [15].

The wide knowledge available on both cyt c structure and its ET properties when assembled on a metal surface can help in designing new devices including cyt c molecules. According to the Marcus theory, the ET process is highly dependent on the distance between the redox centre and the electrode [16–18]. Furthermore, diffusion can reduce the ET efficiency and, thus, its effects should be minimized by immobilizing the protein, with correct orientation optimized for fast electron exchange both with the electrode and the detectable partner. Indeed, the molecular orientation with the haem centre toward the electrode surface favours interfacial ET, even if the same side is usually involved in the docking of partners [19]. Thus, the sensitivity and reliability of cyt c-based hybrid systems are strongly dependent on how the protein is assembled on the support [20].

Good electrical communication can be obtained by direct protein adsorption on a metallic surface, through hydrophobic or electrostatic interaction [21–24], or by exploiting the high affinity for gold of thiols of cysteine residues naturally available or genetically engineered [25–28]. The short distance between the haem centre and the conductive substrate can favour ET, but, apart from an extensive protein–substrate interaction, a loss of electrical signal [29–31] and partial protein denaturation [32–35] might occur at metallic surfaces. The direct interaction of the protein with the metallic surface can be reduced by modifying

the electrode surface with monolayers of short molecules [25, 26, 36–39], which offer the opportunity both to suitably tailor the protein–substrate distance, and to shelter the protein from possible destructive interactions with the metal [2, 36, 39, 40]. In addition, a controllable, well-defined protein immobilization achieved by a linker may increase the protein flexibility, favouring protein recognition and binding to a molecular counterpart.

Besides the widely adopted self-assembled monolayers (SAMs), single-walled carbon nanotubes (SWNTs) are emerging as very powerful linkers, thanks to their peculiar conductive properties and to the significant progresses recently made in both their chemical functionalization and manipulation. Indeed, some examples of metalloproteins and enzymes adsorbed on SWNTs immobilized on metal electrodes have been reported in the literature [41–43].

A key step following the theoretical design and implementation of a hybrid system is its characterization at the single-molecule level, also in view of comparing devices obtained by different immobilization strategies and, then, selecting those with the best features for specific applications. Because of the variety of aspects to be considered (orientation, electric communication, functionality, stability, etc), it is nowadays widely recognized that such a characterization can only be obtained by a joint employment of several suitable techniques, allowing one to define the topology, spectroscopic and electrical properties of the systems at the single-molecule level [33]. The morphological and electrical conductivity of individual metalloproteins immobilized onto gold substrates can be investigated by high-resolution microscopy techniques, such as atomic force microscopy (AFM), scanning tunnelling microscopy (STM) and conductive AFM (CAFM) [44, 45]. In particular, tapping-mode AFM (TMAFM) is largely used for investigating the topology of soft biological material immobilized on solid supports, because it reduces the mechanical perturbations on the imaged sample. Additionally, conductive AFM (CAFM) and STM/STS (scanning tunnelling spectroscopy) allow one to probe the conductive properties of adsorbed single biomolecules, as well as to assess the efficient conduction towards the electrode and through the single molecule [46–48]. This characterization can be integrated with cyclic voltammetry in order to confirm the preserved redox functionality of molecules upon immobilization on gold [44, 49]. Furthermore, cyt c-based hybrid systems can be also investigated by exploiting the potentialities of Raman spectroscopy, which has been shown to selectively probe the spin and oxidation state of haem in cyt c, together with its orientation with respect to the metallic surface [50].

In the present work, various aspects related to immobilization and characterization of cyt c onto gold substrates have been elucidated by focusing our attention on yeast cytochrome c (YCC), a small (12.5 KDa), robust single-domain haem protein, that bears an unique additional free sulfur-containing group (Cys102) located in a region opposite to the haem active site. This cysteine is suitable for tethering the protein onto bare or properly modified gold electrodes, with only minor perturbation of the haem group [44]. In order to provide stable protein immobilization, the integration of YCC with gold has been achieved by using three different organic linkers. Specifically, the thiol of Cys102 is allowed to react with maleimide- and thiol-terminated monolayers assembled on the Au(111) surface. A third immobilization strategy exploits the electrostatic interaction of amine groups of the YCC protein with carboxilic groups on the sidewalls of acid-oxidized SWNTs, adsorbed on a cysteamine-modified Au(111) surface [41, 51, 52]. The resulting hybrid systems have been characterized by scanning probe microscopies and spectroscopies (including Raman spectroscopy), down to the single-molecule level. Finally, the YCC electric conduction with respect to metallic and non-metallic electrodes has been addressed by CAFM. All the results, compared with those obtained for YCC integrated with bare gold, are discussed in view of possible applications of YCC redox protein in nano-bioelectronics.

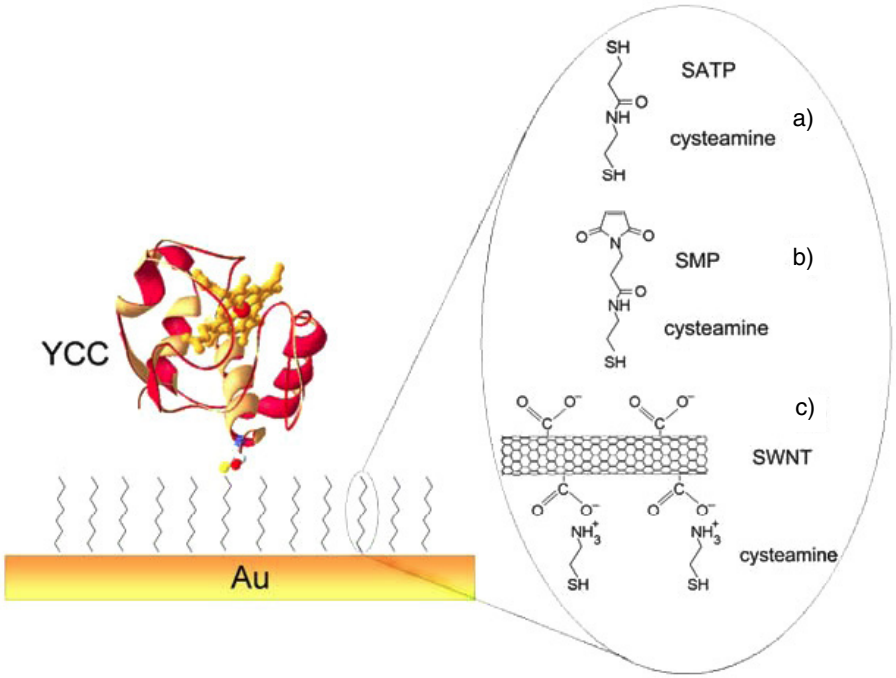

Figure 1. Graphic representation showing YCC adsorbed on (a) SATP-cysteamine-modified, (b) SMP-cysteamine-modified, and (c) SWNT-cysteamine-modified Au(111) substrates.

2. Materials and methods

2.1. Sample preparation

YCC, SWNTs (90% pure) and all chemicals were purchased from Sigma-Aldrich and used without further purification. The gold substrates (Arrandee®) are vacuum-evaporated thin gold films (thickness 200 nm) on borosilicate glass. Prior to experiments, the substrates were flame-annealed to obtain atomically flat Au(111) terraces over hundreds of nanometres. In order to functionalize the annealed Au(111), the substrates were first immersed in an ethanolic solution of cysteamine 1 mM for 15 h at room temperature. Afterward, thiol-terminated monolayers (a), maleimide-functionalized monolayers (b) and acid-oxidized SWNTs (c) were assembled on cysteamine-modified gold substrates in order to exploit different immobilization strategies (see figure 1).

Thiol-terminated alkanethiols were obtained by treating the amino-terminated layer to a solution of N-succinimidyl-S-acetylthiopropionate (SATP) 20 mM, in 10% dimethyl sulfoxide (DMSO) and 90% PBS buffer pH 7 for 2 h at room temperature. Subsequently, the thiol groups of the spacers were deprotected by exposing the sample to hydroxylamine 0.5 M in PBS 50 mM pH 7, ethylenediaminetetraacetic acid (EDTA) 25 mM and dithiothreitol (DTT) 50 mM for 20 min. Samples were then rinsed with Milli-Q water (Millipore 18.2 MΩ).

Maleimide-functionalized monolayers were obtained by incubating the cysteamine-modified gold in a solution of N-succinimidyl 3-maleimidopropionate (SMP) 25 mM in *N*,*N* dimethylformamide (DMF) for 40 min at room temperature. After incubation, the excess of reagent was removed by copiously rinsing the sample with DMF and Milli-Q water.

SWNTs were dispersed on cysteamine-modified gold by exploiting the electrostatic interaction with the positively charged amine termination [53]. In order to increase the electrostatic interaction between the SWNTs and the exposed amine group, the nanotubes were functionalized with–COOH groups on the lateral sides, by an oxidation procedure [54]. SWNT functionalization was obtained by a two-step procedure: 10 mg of SWNT powder were sonicated (50–60 Hz) in 40 ml of a 3:1 mixture of concentrated H_2SO_4:HNO_3 for 20 h and then treated for 30 min with a 4:1 mixture of concentrated H_2SO_4:H_2O_2 (30% aqueous solution) at 70 °C. After each oxidation step, the SWNT acid solution was diluted 1:5 in Milli-Q water and filtered with 0.2 μm pore size polycarbonate filters (Millipore). Finally, the SWNTs were suspended in a mixture of Milli-Q water and NaOH at pH $\sim$ 11 and sonicated for 3 h. Prior to deposition of SWNTs, the cysteamine-modified gold substrate was rinsed with abundant ethanol and Milli-Q water, dried with a pure nitrogen flux and then protonized. The protonization of the amine group was obtained by treating the cysteamine SAM with 0.1 M HCl aqueous solution for 5 min, and then washing it with Milli-Q water and drying in a pure nitrogen flux. Immediately after, 160 μl of 0.4 mg ml^{-1} SWNT aqueous solution were deposited on the modified Au substrate for 2 h; finally the sample was washed with Milli-Q water and dried with pure nitrogen.

The SATP-, SMP- and SWNT-modified gold substrates were incubated with YCC protein solution (30 μM in 30 mM PBS pH 7.0) from one to several hours at room temperature. After protein incubation, the samples were rinsed in Milli-Q water and dried with pure nitrogen flux.

For current–voltage (I–V) measurements, YCC molecules were adsorbed either on bare Au(111) substrates or on gold-coated AFM probes. Standard silicon cantilevers coated with a thin layer of gold with a nominal radius of curvature less than 50 nm and nominal spring constants of 0.05–0.95 N m^{-1} (MikroMash) were used. Gold-coated AFM probes were rinsed with ethanol and Milli-Q water prior to use. Then, they were soaked in protein solution (10 μM YCC in 1 M Tris pH 8.0) for 12–15 h at 4 °C. After incubation, the probes were rinsed with Milli-Q water, blown dry with pure nitrogen and placed in the nanoscope.

2.2. Experimental techniques

AFM topographic images of the surfaces were recorded with a Nanoscope IIIa/Multimode SPM (Digital Instruments) equipped with a 12 μm scanner operating in tapping mode (TM). Oxide-sharpened silicon nitride probes (Digital Instruments), 100 or 200 μm long, with nominal radius of curvature of 10 nm and spring constants of 0.15 and 0.57 N m^{-1}, respectively, were used for all the measurements performed in liquid. Silicon probes (Digital Instruments), 115–135 μm long, with a spring constant of 20–80 N m^{-1} were used for measurements in air. Resonance peaks in the frequency response of the cantilever were chosen for the TM oscillation, corresponding to typical tapping frequencies in the range 8–30 kHz in fluid and 200–300 kHz in air. Free oscillation of the cantilever was set to have a root-mean-square amplitude corresponding to $\sim$1.5 V. In each measurement, the set point was adjusted before scanning, to minimize the tip–sample interaction forces.

Imaging in liquid was performed in Milli-Q water using an open fluid cell (Digital Instruments).

Constant current mode STM images were acquired with both a Picoscan system (Molecular Imaging Co.) equipped with a 10 μm scanner with a final preamplifier sensitivity of 1 nA V^{-1} and a Nanoscope IIIa/Multimode SPM (Digital Instruments). STM tips were prepared by mechanically cutting Pt/Ir wires (Goodfellow).

I–V measurements as a function of the applied force load were carried out by using a CAFM (PicoSPM, Molecular Imaging), equipped with a current-sensing module with a

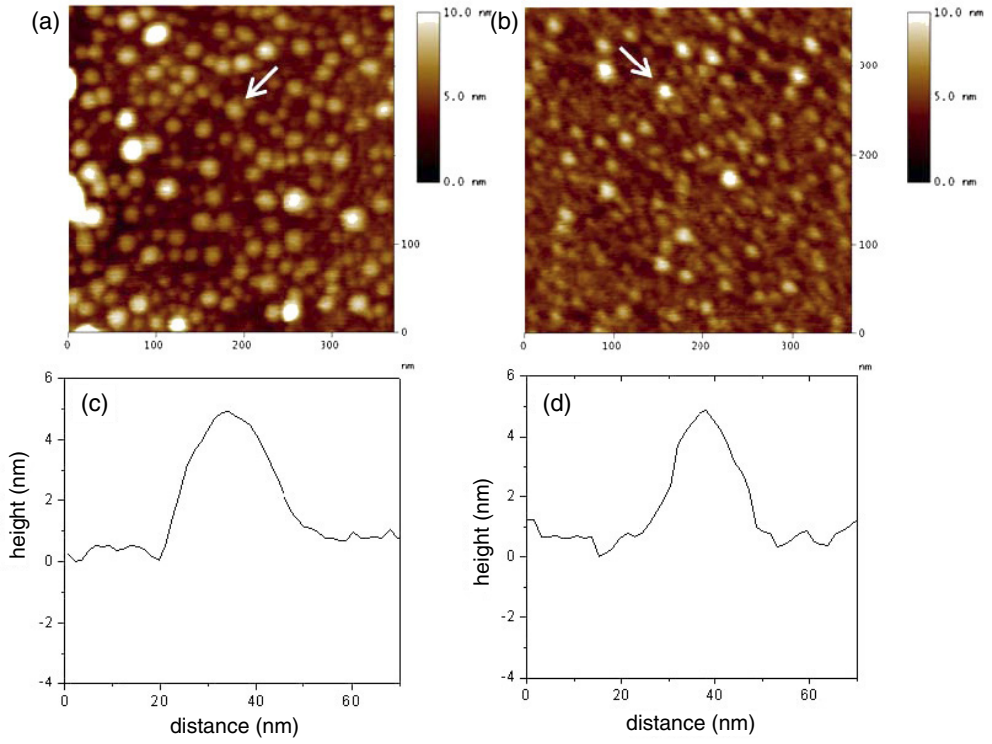

Figure 2. TMAFM images of YCC molecules adsorbed on (a) cysteamine-SATP-modified Au(111) and (b) cysteamine-SMP-modified Au(111) recorded in Milli-Q water. Panels (c) and (d) show the cross-section profiles of molecules indicated by the white arrows in (a) and (b), respectively.

sensitivity of 1 nA V^{-1} (operational range from few pA to 10 nA). Each single I–V sweep was registered in 0.3–0.5 s. The measurements were done at room temperature, and pure nitrogen gas was flushed in the environmental chamber of measurements.

Scanning probe microscopy measurements were carried out in liquid and in air in order to test the stability of the hybrid systems in the two experimental conditions.

Raman spectra were recorded using two confocal micro-Raman systems. The first one (Jobin-Yvon, Super Labram) was equipped with a liquid-nitrogen-cooled CCD detector (EEV CCD10-11 back illuminated; pixel format: 1024 × 128) and an argon-ion laser providing a 514 nm radiation. The second micro-Raman system (Jobin-Yvon, Labram) was equipped with a Peltier-cooled detector and a HeNe laser with an excitation wavelength of 633 nm. In both cases a spectrograph with a 1800 g mm^{-1} grating and a 100× objective allowing a resolution of about 5 cm^{-1} were used. The laser power was kept below 4 mW.

3. Results and discussion

3.1. YCC immobilized on thiol- and maleimide-functionalized Au(111) electrodes

3.1.1. AFM measurements. Topographic images of YCC molecules immobilized on thiol- and maleimide-modified gold substrates, as measured by TMAFM in Milli-Q water, are shown in figures 2(a) and (b), respectively for an incubation time of about 1 h. Similar images have been recorded on different areas of the samples, revealing a uniform distribution of the adsorbed

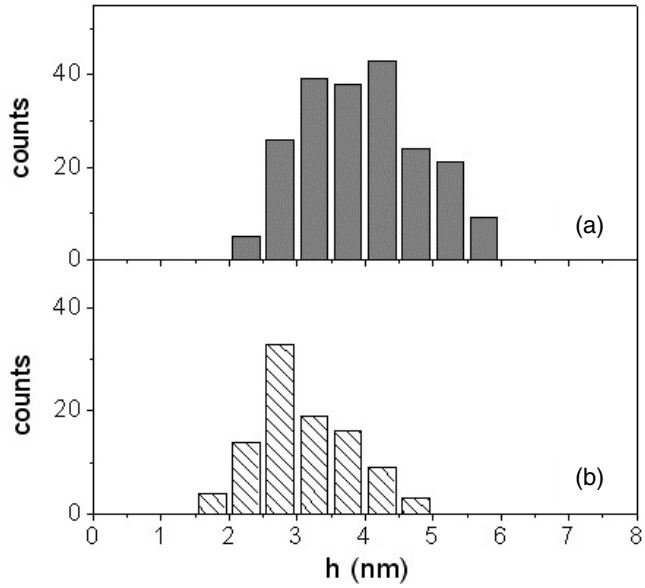

Figure 3. Statistical distributions of YCC molecular height over (a) cysteamine-SATP-modified and (b) cysteamine-SMP-modified Au(111) substrates, as estimated from 220 and 100 individual cross-section profiles, respectively. Mean heights resulting from distributions: 3.9 ± 0.9 nm (a) and 3.1 ± 0.7 nm (b).

proteins. The molecules display homogeneous lateral and vertical dimensions. Additionally, the imaged metalloproteins do not reveal mobility over the modified gold, as derived by high-quality images even after repetitive scans. The density of YCC molecules on thiol- and maleimide-modified gold substrates can be modulated from very low to full coverage by a suitable choice of incubation time. Similar results have been found even by acquiring TMAFM images in 30 mM PBS pH 7.0 buffer solution.

The histograms of protein heights, measured from several (more than 80) single-molecule cross-section profiles (see figures 2(c) and (d)), are shown in figure 3. The distributions of the measured height are monomodal and centred at (3.9 ± 0.9) and (3.1 ± 0.7) nm for the thiol- and for the maleimide-terminated monolayer, respectively. These values well match the vertical height of the protein corresponding to non-denaturing immobilization of YCC through the sulfur atom of the Cys102 residue (evaluated to be about 3.8 nm, from the crystallographic data) [44, 55]. This suggests that the protein molecules adopt a standing-up configuration over both the modified gold substrates. Moreover, we notice that the mean heights are in both the cases greater than the height of YCC molecules directly adsorbed on bare gold surfaces (2.6 ± 0.7 nm [44]). This is in agreement with the results found for the copper protein azurin [56]. In that case, the vertical dimension changed from (1.7 ± 0.5) nm, for immobilization on bare gold, to (3.4 ± 0.5) nm when immobilization is achieved via a thiol-terminated alkanethiol spacer, the expected vertical value from crystallography being 3.1 nm [34]. Such a result therefore indicates that the interactions of metalloproteins with the noble metal surfaces can be reduced by the presence of spacers. Additional information on protein arrangement on the surfaces can be obtained from the width of height distributions, which can be associated with flexibility of the protein on the substrate. Actually, a higher probability of different protein orientations can be reflected into a broader height distribution [44, 47, 57]. The evidence that the standard

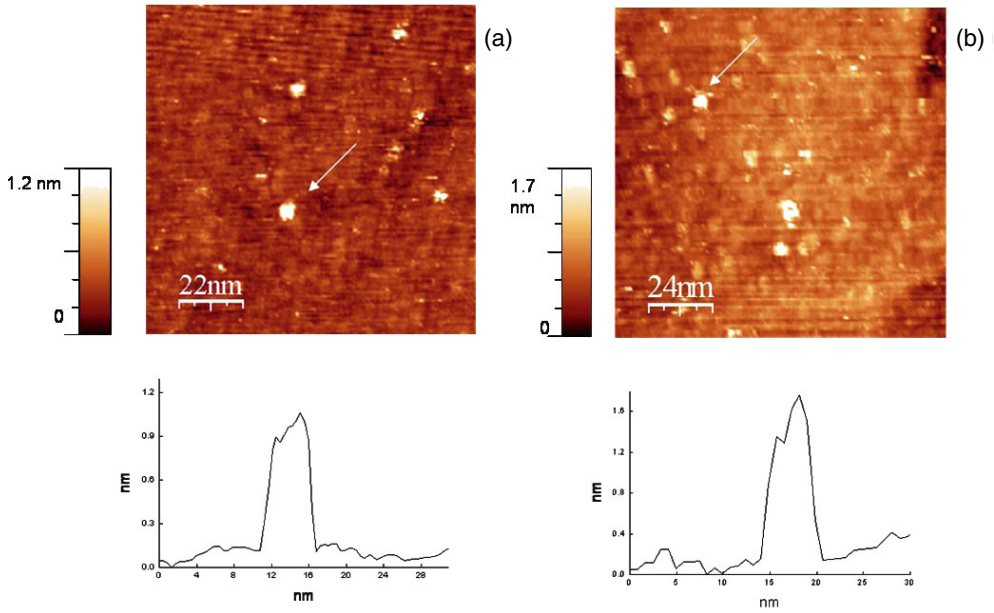

Figure 4. Constant current mode STM images of YCC molecules immobilized on thiol-terminated (a) and on maleimide-terminated (b) monolayers assembled on Au(111) substrates. Cross-section profiles of the molecules indicated by the arrows are shown below. The images have been acquired in air at a tunnelling current of 40–50 pA and at bias of −0.6 and −0.8 V, respectively.

deviations estimated for YCC molecules adsorbed both on thiol- and maleimide-terminated monolayers (0.9 and 0.7 nm, respectively) are similar to those found for YCC anchored through Cys102 onto bare gold (0.7 nm [44]) suggests comparable flexibilities of the molecules on the substrates, likely with higher flexibility when a thiol-terminated linker is employed.

Minor information can be obtained from AFM images about the lateral dimensions of the proteins. The relatively large size of the AFM tip and its geometry induce broadening effects, and an estimation of the lateral dimensions can be evaluated by deconvolving the imaged molecules with the tip shape [58] considering, at a first approximation, the imaged objects as spherical. For a tip with radius of curvature r, the diameter d of the object is given approximately by $d = W^2/(8r)$ [58], where W is the measured apparent width. In our experiment the nominal tip radius is 10 nm and the average apparent widths W are in the range 20–30 nm, so that we obtain for the lateral size of adsorbed YCC d values of about 4 nm for thiol-terminated monolayers and 3 nm for maleimide-terminated monolayers. These values are consistent, within the errors (around 25%), with each other and with the corresponding molecular heights, as previously discussed.

3.1.2. STM measurements. Representative constant current STM images of YCC molecules immobilized on either thiol-terminated (figure 4(a)) or maleimide-terminated (figure 4(b)) monolayers assembled on Au(111) surfaces are shown in figure 4; single YCC molecules are well resolved on both substrates. Furthermore, they are stable, giving reproducible images in consecutive scans. This can be presumably due to strong interactions as achieved by the covalent bond between the molecule and the substrate. Accordingly, previous STM measurements demonstrated that single YCC molecules, as well as other metalloproteins,

are chemisorbed onto bare gold surfaces via the exposed Cys residues [33, 44]. Conversely, previous measurements showed that repeated scans with the STM tip remove protein molecules that are not non-covalently immobilized on the electrode [44, 59, 60].

An analysis of the molecular lateral size (see as an example the cross-section profile of figure 4) gives an average value of 4.9 ± 1.1 nm for YCC over thiol-terminated surfaces, close to that obtained from x-ray crystallography [55] and in a good agreement with that observed for the protein directly adsorbed on gold (4.8 ± 0.7 nm) [44]. On the other hand, the molecular lateral size of YCC on maleimide-terminated monolayers is found to be slightly higher than that obtained on thiol-terminated monolayers (6.2 ± 0.1 nm). This larger value could be likely related to a modification of the charge distribution around the protein as induced by interaction of the protein with the maleimide-terminated monolayer [61]. Indeed, other hypotheses, such the formation of dimers or a partial denaturation, can be ruled out on the basis of the AFM morphology analysis revealing the presence of well-defined single YCC molecules.

The cross-section analysis gives a YCC molecular height of 0.8 ± 0.1 nm on maleimide-terminated monolayers and of 1.1 ± 0.6 nm on thiol-terminated monolayers. Both these values are lower than the crystallographic one, but higher than the height obtained for YCC directly adsorbed on gold (0.3–0.5 nm) [44]. An analogous increment in the protein vertical size, as compared to bare gold, has been detected from STM images of azurin chemically anchored to SATP-cysteamine-modified gold [56]. Indeed, an underestimation of physical height is a general feature of STM images of biomolecules directly assembled on conductive substrates [44, 47, 61–65], and it is likely related to the low conductivity of biomolecules. However, in STM images, obtained operating in constant current mode, an increment in the molecular height (namely, in the registered tunnelling current) of metalloproteins adsorbed on spacers as compared to bare gold can reasonably reflect differences in electronic conductivity. Accordingly, a more efficient tunnelling current flow through the YCC protein occurs when covalent immobilization is achieved via both thiol- and maleimide-terminated spacers.

3.2. YCC on carbon nanotubes adsorbed on cysteamine-modified Au(111)

3.2.1. AFM measurements. Representative TMAFM images of –COOH-functionalized SWNTs assembled on cysteamine-modified gold substrate are reported in figures 5(a) and (b) (topography and corresponding amplitude modulation, respectively). The nanotube feature imaged in figure 5(a) is well resolved on the substrate. It has a vertical size of 2.8 nm and a length of 250 nm. Repetitive scans of large areas show that the SWNTs are homogeneously distributed on the substrate and stably bound to modified gold.

A statistical analysis over 85 SWNTs reveals a mean height of (4.4 ± 1.7) nm and a mean length around 200 nm. Taking into account that the nominal SWNT diameter ranges from 0.8 to 1.6 nm and their nominal length is about 500 nm, these results indicate that imaged SWNTs are mainly grouped in bundles and that they have been shortened by the sonication treatment in acid ambient. A few globular structures are occasionally observed on SWNTs, with a mean occurrence of 0.65 per nanotube. Examples are shown in figures 5(a) and (b) (see arrows). A statistical analysis performed on their vertical size, by cross-section profiles, shows a mean height of 5.5 ± 3.9 nm, with a broad distribution.

After incubation with YCC, the carbon nanotubes appear decorated by several globular structures, as shown in the TMAFM topography image (figure 5(c)) and, more clearly, in the corresponding amplitude modulation image (figure 5(d)). These globular structures can be ascribed to adsorbed YCC molecules, in agreement with previous works demonstrating successful protein immobilization via the electrostatic interaction between the –COOH groups present on the SWNTs sidewalls and the lysine residues of the proteins [41, 51, 52]. YCC

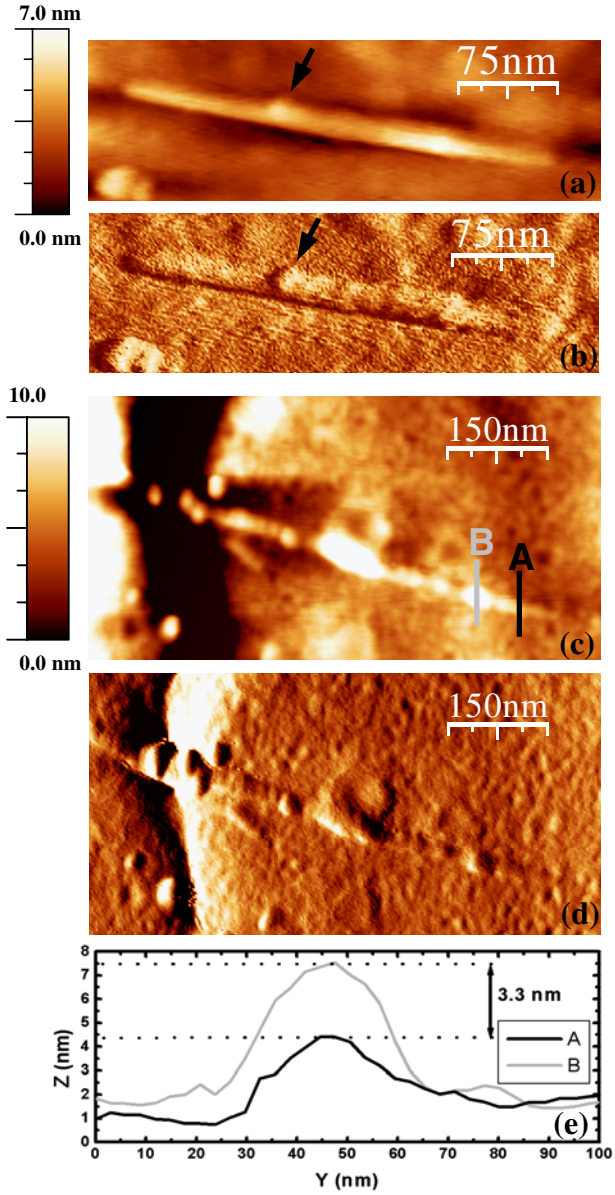

Figure 5. (a) Topographic and (b) amplitude modulation images of a bundle of functionalized SWNTs adsorbed on modified Au(111) terraces before the YCC incubation, as recorded by TMAFM in air. The same ((c) topographic and (d) amplitude) images after the YCC incubation. (e) Cross-sections highlighted in figure 5(d): SWNTs bundle without (A) and with (B) a YCC molecule.

molecules appear stably bound to SWNTs, since they are imaged after sample rinsing and remain unperturbed after repetitive scans.

By imaging different areas of the sample, we found that the number of YCC molecules per nanotube ranges from 1 to 10, with a mean value of 5, significantly higher than that related to the globular objects found before YCC incubation. Cross-sections of the bare part

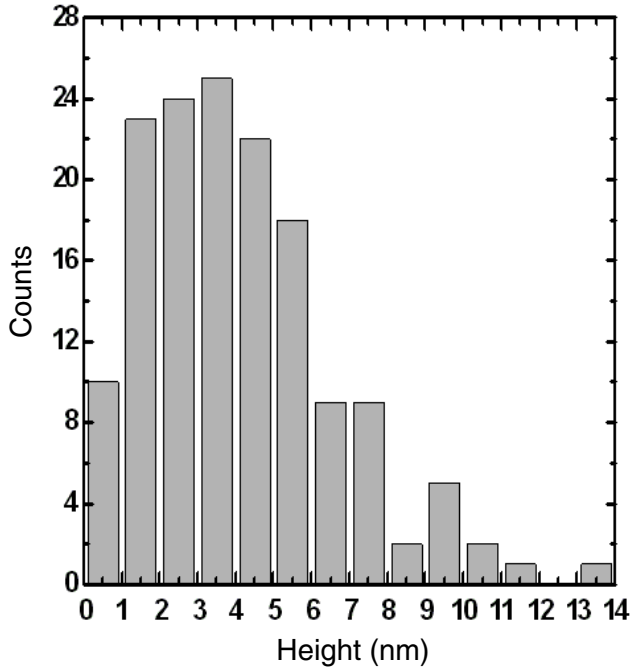

Figure 6. Statistical analysis of the height of YCC molecules adsorbed on acid-oxidized SWNTs, as evaluated from TMAFM imaging in air over 30 SWNTs (150 objects). Resulting mean value of 3.7 ± 1.9 nm.

of a nanotube (A, black bar in figure 5(c)) and of a protein adsorbed on the same nanotube (B, grey bar in figure 5(c)) are shown in figure 5(e). The YCC height is estimated from the difference between the maximum values of the vertical size of the two cross-sections (3.3 nm in figure 5(e)). The statistical analysis, on 30 different nanotubes, provides a distribution of the molecular height peaked at 3.7 ± 1.9 nm, corresponding to the histogram reported in figure 6. The agreement between the mean height of the structures present after YCC incubation with the crystallographic size of YCC as for non-denaturated adsorption [44, 55] further confirms that YCC molecules have been effectively bound to SWNTs. Moreover, the standard deviation is much higher than those obtained for YCC chemisorbed on monolayer-modified or bare gold substrates [44, 47], and this could reflect some heterogeneity in the molecular orientation of YCC onto SWNTs, as expected for a non-specific, electrostatic interaction.

3.2.2. Raman measurements. In figure 7(a), a typical spectrum obtained for bare SWNTs on cysteamine-modified Au substrate with 514 nm excitation is shown; the Raman fingerprints of SWNTs are clearly detected. In particular, bands at 1350 and 1593 cm^{-1}, corresponding to disordered carbon (D band) and out-of-phase graphene sheet-like vibration (G band), [66–68], respectively, are disclosed. Similarly, by 633 nm excitation, these peaks occur at 1330 and 1591 cm^{-1} (see the inset of figure 7(a)). Such a shift of the D band toward lower frequencies as the excitation wavelength increases is a well-known effect related to the selective coupling of the incident light with the strong optical electronic transitions [69]. The ratio of the intensity of the G and D bands, representative of 'defects' in SWNTs, around 3, suggests that the SWNTs have actually been functionalized [70, 71]. The low-frequency region, available only

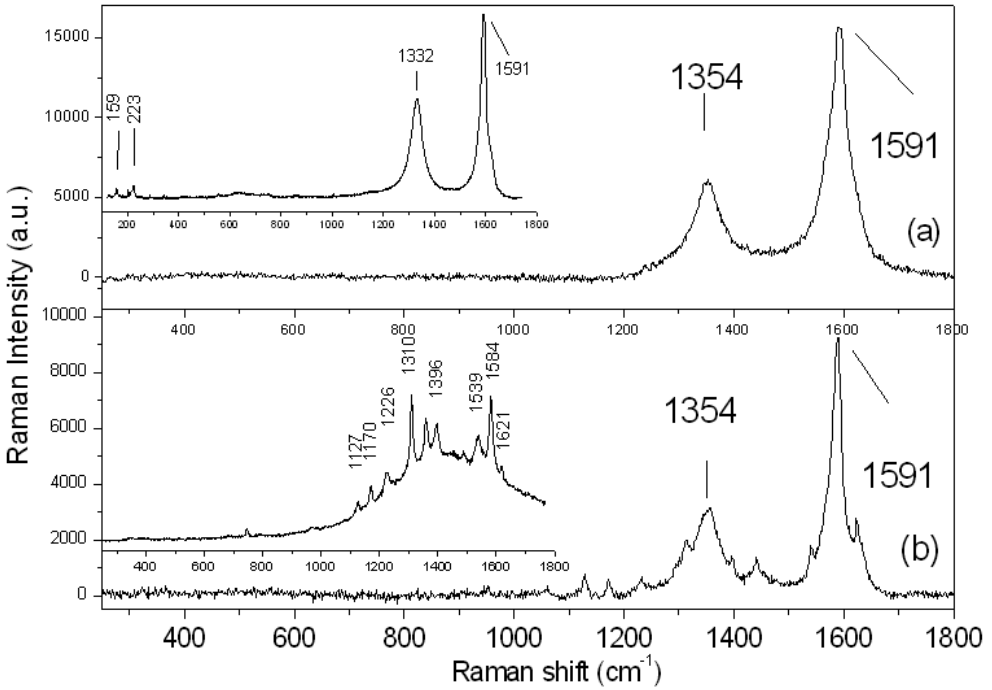

Figure 7. Raman spectra obtained with a 514 nm excitation wavelength for various samples. (a) Functionalized SWNTs on cysteamine-modified Au substrate at 514 nm excitation wavelength; inset: the same at 633 nm excitation wavelength. (b) YCC on functionalized SWNTs (see text); inset: dry YCC sample deposited on glass [75].

for the 633 nm excitation, shows two bands located at 159 and 223 cm^{-1}, corresponding to radial breathing modes (RBMs), [66–68]. Their positions can be used to estimate the SWNT diameter [66, 72–74], which results to be around 0.9 nm, in agreement with the nominal value.

A representative Raman spectrum ($\lambda_{ex} = 514$ nm) of the sample after YCC incubation is shown in figure 7(b). Superimposed on the SWNT spectrum, well-defined peaks are observed at 1127, 1170, 1226, 1310, 1396, 1539, and 1621 cm^{-1}, which recall the YCC Raman features (see the inset of figure 7(b) for comparison) arising from the inner and outer ring stretching vibrations of the haem [50, 75]. The G/D intensity ratio is unchanged with respect to that found before YCC incubation, as expected for electrostatic interaction between the proteins and SWNT [41, 70]. The intensities of YCC Raman features are slightly different from site to site; sometimes, the SWNT features are hidden by the YCC Raman spectrum. Such a dependence of Raman spectra on the site reflects the variability in the number of YCC molecules onto SWNTs evidenced also by TMAFM measurements. On the other hand, Raman measurements performed on YCC directly adsorbed onto cysteamine-modified gold substrates reveal a very weak signal.

Concerning the spin marker modes of YCC, lines corresponding to the high-spin state (1539, ν_{11}, and 1621 cm^{-1}, ν_{10}) are detected in figure 7(b), suggesting that the preferred (or more probable) haem configuration of YCC on functionalized SWNTs is the one with high-spin 5 coordinate [50]; this is similar to that found for YCC in the proximity of an Ag surface [75, 76].

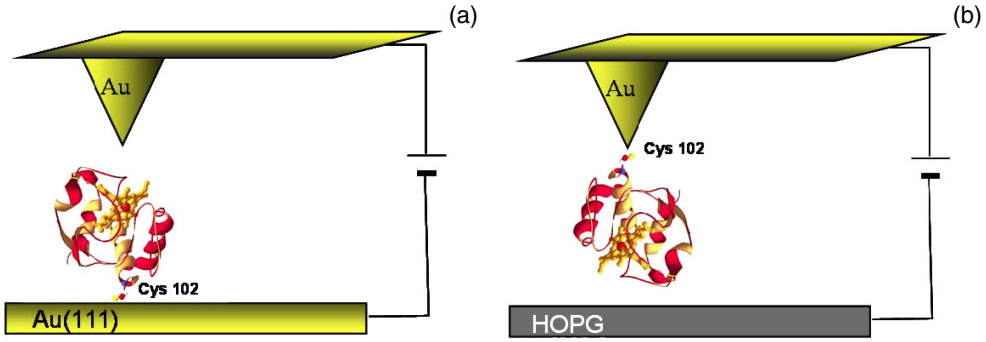

Figure 8. Scheme of the Au/YCC–Au (a) and the Au–YCC/HOPG (b) junctions.

3.3. Molecular conduction of YCC

Molecular conduction of a YCC protein molecule sandwiched within two nanojunctions has been achieved by using CAFM. Specifically, in a first junction, YCC is chemisorbed via its free cysteine Cys102 on an Au(111) substrate and physically contacted by a gold-coated AFM probe (see figure 8(a)). Such a junction is hereafter indicated by Au/YCC–Au. In a second junction (see figure 8(b)), the YCC is chemically anchored to a gold-coated AFM probe and brought against a highly oriented pyrolytic graphite (HOPG) substrate, establishing a physical contact with it. This latter configuration has been called Au–YCC/HOPG.

In both biomolecular junctions, by varying the voltage between ± 2 V, the current response of the metalloprotein is monitored, along with the effect on molecular conductance of the compressive vertical forces. In figure 9(a), I–V curves, recorded when the gold tip is brought into contact with YCC molecules adsorbed on an Au(111) substrate (i.e., Au/YCC–Au nanojunction), are shown for different force loads. At 2 nN, a low current response is observed, while a small increment of the applied force (4 nN) determines a large current response, saturating the preamplifier limit (± 10 nA), in the bias region outside the interval ± 1 V. In contrast, when bare gold-coated tips are brought into physical contact with a bare Au(111) substrate, a high ohmic current response (that saturates the 10 nA preamplifier) is observed, independently of the applied force load. The I–V characteristics are found to be reproducible on different areas of the samples.

In the Au–YCC/HOPG junction, the YCC-modified gold tip, brought in physical contact with the HOPG substrate, appears almost electrically insulated for a force load ranging between 2 and 20 nN (data not shown). The I–V measurements are then repeated by using stiff cantilevers (spring constant values in the range 0.60–0.95 N m^{-1}) in order to apply higher force loads. In figure 9(b), the I–V characteristics of a YCC-modified gold-tip in contact with the HOPG electrode are shown, when raising the applied force load in the range 30–86 nN. For an applied load of 30 nN, an appreciable I–V response is obtained. In contrast to what is observed for the Au/YCC–Au junction, the current signal slowly increases with higher forces, especially in the bias region outside ± 1 V. For low biases a very small conduction is observed, even for a high force load (86 nN). When withdrawing the YCC-modified AFM probe and approaching it again to the HOPG electrode, the I–V curves are very similar to those obtained with bare tips against the HOPG surface: a high ohmic current response saturating the preamplifier limit is observed, independently of the applied force load. This means that, when the force load exceeds 80 nN, the protein is removed from the probe and a direct electrical contact with the underlying surface is attained.

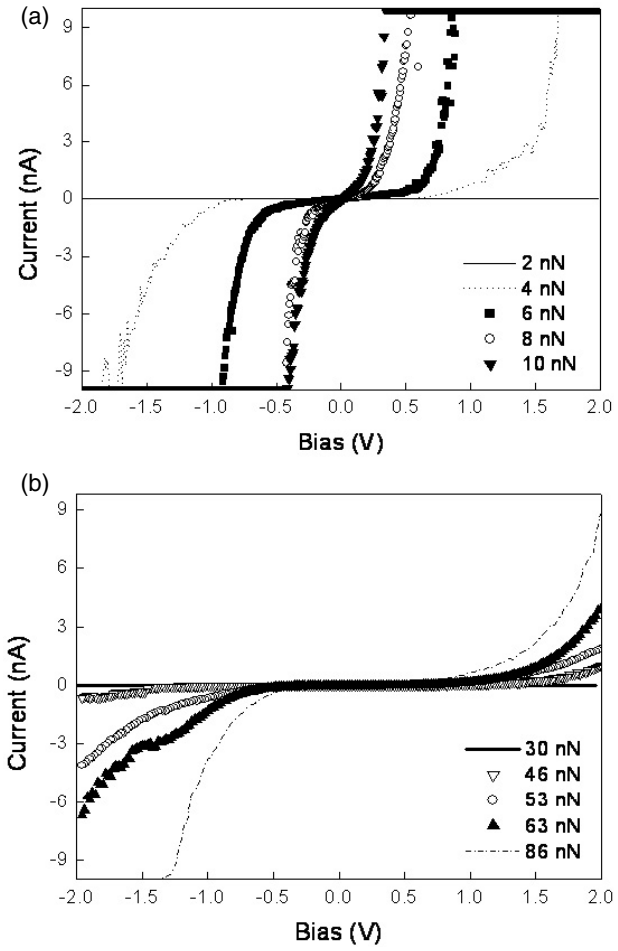

Figure 9. I–V curves, at increasing applied force loads, recorded under nitrogen atmosphere, on (a) YCC chemisorbed on Au(111) by means of a gold-coated AFM probe (i.e. Au/YCC–Au nanojunction) and (b) when a YCC-modified gold-coated tip is brought in physical contact with the HOPG substrate (i.e. Au–YCC/HOPG nanojunction).

These I–V characteristics are found to be reproducible by using several tips. The behaviour of the Au–YCC/HOPG junction seems to indicate that higher contact force applied by stiff cantilevers can establish a more stable and reliable electric contact between the protein and the HOPG electrode.

The difference in the electrical behaviour of the two junctions suggests a dramatic dependence of nanojunction conductive features on the electrode materials. However, the junction configuration (namely, immobilization of the protein on tip or on substrate) could play some role, too. Thus, to test the effect of junction configuration is a fundamental aspect for a better understanding of our results. With this aim, I–V measurements have been performed by bringing the YCC-modified gold tip against a bare Au(111) substrate. In figure 10, the I–V curves obtained on applying various force loads in the range 13–27 nN are shown. An appreciable current can be registered at an applied load of 13 nN; the current increases when raising the force and a high current signal (saturating the preamplifier limit) is observed at

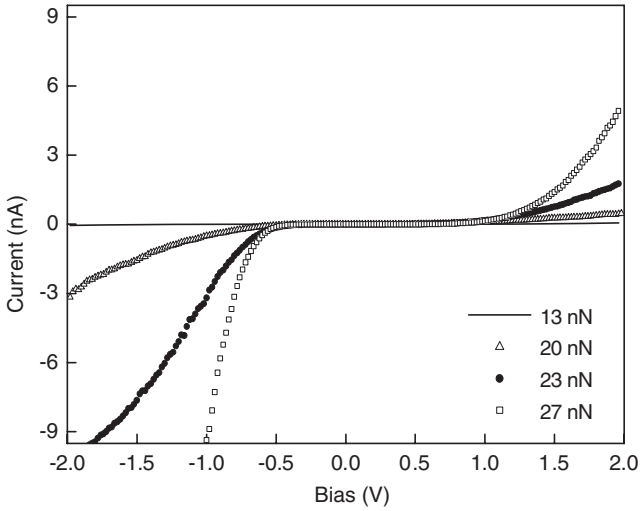

Figure 10. *I–V* curves, at increasing applied force loads, recorded under nitrogen atmosphere, on a YCC-modified gold-coated tip brought into physical contact with the Au(111) substrate.

23–27 nN, but only for bias around −1 V. This asymmetric behaviour was not observed for the Au/YCC–Au nanojunction having the YCC bound onto flat Au(111) surface. In principle, this difference could be due either to the asymmetric positioning of the redox centre in the Au–YCC/Au junction, or to a different nature of the contact at the tip–molecule and substrate–molecule interfaces [77]. This asymmetry was not observed for the other two junctions investigated here; thus this aspect requires further investigations.

Importantly, these results indicate that the physical contact established with the protein by the gold tip or by the flat Au(111) surface is slightly different, but it cannot be responsible for the significant difference in the electrical behaviour of the Au/YCC–Au and Au–YCC/HOPG junctions. Actually, the minimum force loads providing a current response for the Au/YCC–Au junctions with different YCC configurations (2 or 13 nN, for YCC on the gold tip or on flat gold, respectively) are still lower than that required for an Au–YCC/HOPG junction (30 nN). More likely, this can be related to the characteristics of the junction, namely the electrode material and nature of contacts. The electron transport through a protein-based junction can be viewed as a coherent electron tunnelling, where the total conductance across the junction can be given by the product of the conductance of contacts and of the molecule [78, 79], and some authors have demonstrated that the contact resistance decreases with increasing work function of the electrodes in physical contact with the molecule [80]. Thus, the difference in minimum applied forces can reasonably be due to the lower work function of HOPG (4.65 eV) compared to that of gold (5.10 eV) [80, 81].

These results point out that the choice of electrode material and of the nature of the contacts between protein and electrodes are crucial issues in obtaining good electron transport nanojunctions.

4. Conclusions

The integration of the ET protein YCC with conductive electrodes has been deeply investigated down to the single-molecule level, with the aim of elucidating those aspects relevant to applications of hybrid systems in nano-biotechnology.

YCC has been successfully integrated with modified gold electrodes by exploiting both covalent (either with maleimide- or thiol-terminated monolayers) and electrostatic binding (carbon nanotubes). Each hybrid system has been characterized by TMAFM, and the analysis of molecular heights supports YCC non-denaturing adsorption in the three immobilization strategies proposed. TMAFM measurements reveal multiple orientations of YCC on functionalized SWNTs, whereas Raman spectroscopy discloses a preferential high-spin 5 coordinate haem configuration. A standing-up arrangement of the protein for covalent binding is suggested, together with a higher protein flexibility provided by the thiol-terminated monolayer. Moreover, STM measurements show that the use of maleimide- and thiol-terminated short spacers allows a good electric coupling of the protein with the gold electrode, facilitating the tunnelling process through the YCC protein, as compared with YCC adsorbed on bare Au(111).

This comprehensive multi-technique approach demonstrates that, by using suitably functionalized organic linkers for stable protein immobilization on gold, the native form of the protein can be preserved and its flexibility guaranteed; these aspects are fundamental for recognizing and binding the molecular counterparts.

The investigation of two YCC-based nanojunctions has been carried out by CAFM. Molecular conduction of a single YCC molecule in contact with either a metallic (gold) or non-metallic (HOPG) electrode results in being facilitated when YCC is adsorbed on a flat Au(111) substrate and contacted by a gold tip, with an appreciable current flow even at low applied forces (2 nN). These results open new perspectives for the integration of single redox proteins with gold electrodes, which are worth exploring fully. The conduction properties of junctions with YCC in contact with modified gold electrodes are currently under investigation.

Acknowledgments

This work has been partially supported by the FIRB-MIUR Project ‘Molecular Nanodevices’ and PRIN-MIUR 2006 projects (no. 2006028219 and 2006027587). Thanks are due to Dr Melinda Lakatos for her preliminary measurements on SWNTs. L Andolfi acknowledges the Research Grant MIUR ‘Rientro dei Cervelli’.

References

[1] Willner I, Katz E and Willner B 1997 *Electroanalysis* **9** 965
[2] Willner I and Katz E 2000 *Angew. Chem. Int. Edn* **29** 1180
[3] Göpel W and Heiduschka P 1995 *Biosens. Bioelectron.* **10** 853
[4] Schuhmann W 1995 *Biosens. Bioelectron.* **10** 181
[5] Gilardi G and Fantuzzi A 2001 *Trends Biotechnol.* **19** 468
Gilardi G, Fantuzzi A and Sadeghi S J 2001 *Curr. Opin. Struct. Biol.* **11** 491
[6] Gittins D I, Bethell D, Schiffrin D J and Nichols R J 2000 *Nature* **408** 67
[7] Shipway A N and Willner I 2001 *Acc. Chem. Res.* **34** 421
[8] Loppacher Ch, Guggisberg M, Pfeiffer O, Meyer E, Bammerlin M, Lüthi R, Schlittler R, Gimzewski J K, Tang H and Joachim C 2003 *Phys. Rev. Lett.* **90** 066107
[9] Xiao Y, Patolsky F, Katz E, Hainfeld J F and Willner I 2003 *Science* **299** 1877
[10] Sigfridsson K, Ejdeback M, Sundahl M and Hasson O 1998 *Arch. Biochem. Biophys.* **351** 197
[11] Haehnel W, Jansen T, Gause K, Klösgen R B, Stahl B, Michl D, Huvermann B, Karas M and Hermann R G 1994 *EMBO J.* **13** 1028
[12] Holm R H, Kennepohl P and Solomon E I 1996 *Chem Rev.* **96** 2239
[13] McNeil C J, Smith K A, Ballavite P and Bannister J V 1989 *Free Rad. Res. Comms.* **7** 89
Fabian R H, De Witt D S and Kent T A 1995 *J. Cereb. Blood Flow Metab.* **15** 242
Song M I, Bier F F and Scheller F W 1995 *Bioelectrochem. Bioenerg.* **38** 419

[14] Waibel M, Schulze H, Huber N and Bachman T T 2006 *Biosens. Bioelectron.* **21** 1132
Chang S-C, Pereira-Rodrigues N, Henderson J R, Cole A, Bedioui F and McNeil C J 2005 *Biosens. Biolelectron.* **21** 917
[15] Bonanni B, Kamruzzahan A S M, Bizzarri A R, Rankl C, Gruber H J, Hinterdorfer P and Cannistraro S 2005 *Biophys. J.* **89** 2783
[16] Moser C C, Keske J M, Warncke K, Farid R S and Dutton P L 1992 *Nature* **366** 796
[17] Bizzarri A R and Cannistraro S 2005 *Encyclopedia of Condensed Matter Physics* (Amsterdam: Elsevier)
[18] Marcus R A and Sutin N 1985 *Biochim. Biophys. Acta* **811** 265
[19] Zhou J, Zheng J and Jiang S 2004 *J. Phys. Chem.* B **108** 17418
[20] Katz E, Heleg-Shabtai V, Willner B, Willner I and Bückmann A F 1997 *Bioelectrochem. Bioenerg.* **42** 95
[21] Willner I and Willner B 2001 *Trends Biotechnol.* **19** 222
[22] Willner I 2002 *Science* **298** 2407
[23] Sagara T, Niwa K, Sone A, Hinnen C and Niki K 1990 *Langmuir* **6** 254
[24] Taniguchi I, Watanabe K, Tominaga M and Hawkridge F M 1992 *J. Electroanal. Chem.* **333** 331
[25] Weisshaar D E, Lamp B D and Porter M D 1992 *J. Am. Chem. Soc.* **114** 5860
[26] Ulman A 1996 *Chem. Rev.* **96** 1533
[27] Nuzzo R G, Zegarski B R and Dubois L H 1987 *J. Am. Chem. Soc.* **109** 733
[28] Grönbeck H, Curioni A and Andreoni W 2000 *J. Am. Chem. Soc.* **122** 3839
[29] Zhou Y, Nagaoka T and Zhu G 1999 *Biophys. Chem.* **79** 55
[30] Reed D E and Hawkridge F M 1987 *Anal. Chem.* **59** 2334
[31] Armstrong F A 1990 *Struct. Bond.* **72** 137
[32] Davis J J and Hill H A O 2002 *Chem. Commun.* **5** 393
[33] Bonanni B, Alliata D, Andolfi L, Bizzarri A R and Cannistraro S 2005 *Surface Science Research Developments* ed C P Norris (New York: Nova Science) p 1
[34] Bizzarri A R, Andolfi L, Stchakovsky M and Cannistraro S 2005 *J. Nanotechnol.* **1** 100
[35] Schnyder B, Koetz R, Alliata D and Facci P 2002 *Surf. Interface Anal.* **34** 40
[36] Chi Q, Zhang J, Andersen J E T and Ulstrup J 2001 *J. Phys. Chem.* B **105** 4669
[37] Tarlov M J and Bowden E F 1991 *J. Am. Chem. Soc.* **113** 1847
[38] Gaigalas A K and Niaura G 1997 *J. Colloid Interface Sci.* **193** 60
[39] Cavalleri O, Natale C, Stroppolo M E, Relini A, Cosulich E, Thea S, Novi M and Gliozzi A 2000 *Phys. Chem. Chem. Phys.* **2** 4630
[40] Madoz J, Kuznestov B A, Medrano F J, Garcia J L and Fernandez V M 1997 *J. Am. Chem. Soc.* **119** 1043
[41] Azamian B R, Davis J J, Coleman K S, Bagshaw C B and Green M L H 2002 *J. Am. Chem. Soc.* **124** 12664
[42] Itkis M E, Borondics F, Yu A and Haddon R C 2006 *Science* **312** 413
[43] Gooding J J, Wibowo R, Liu J, Yang W, Losic D, Orbons S, Mearns F J, Shapter J C and Hibbert D B 2003 *J. Am. Chem. Soc.* **125** 9006
[44] Bonanni B, Alliata D, Bizzarri A R and Cannistraro S 2003 *Chem. Phys. Chem.* **4** 1183
[45] Nazin G V and Qui X H 2003 *W. Hom. Sci.* **302** 77
Castner D G and Ratner B D 2002 *Surf. Sci.* **500** 28
[46] Andolfi L and Cannistraro S 2005 *Surf. Sci.* **598** 68
Lukins P B and Oates T 1998 *Biochim. Biophys. Acta* **1409** 1
[47] Andolfi L, Bonanni B, Canters G W, Verbeet M Ph and Cannistraro S 2003 *Surf. Sci.* **530** 181
[48] Andolfi L, Canters G W, Verbeet M Ph and Cannistraro S 2004 *Biophys. Chem.* **107** 107
[49] Andolfi L, Bruce D, Cannistraro S, Canters G W, Davis J J, Hill H A O, Crozier J, Verbeet M Ph, Wrathmell C L and Astier Y 2004 *J. Electroanal. Chem.* **565** 21
[50] Hu S, Morris I K, Singh J P, Smith K M and Spiro T G 1993 *J. Am. Chem. Soc.* **115** 12446
Macdonald I D G and Smith W E 1996 *Langmuir* **12** 706
Eng L H, Schlegel V, Wang D, Neujahr H Y, Stankovich M T and Cotton T 1996 *Langmuir* **12** 3055
Wackerbarth H and Hildebrandt P 2003 *Chem. Phys. Chem.* **4** 714
[51] Davis J J, Coleman K S, Azamian B R, Bagshaw C B and Green M L H 2003 *Chem. Eur. J.* **9** 3732
[52] Kam N W S and Dai H 2005 *J. Am. Chem. Soc.* **127** 6021
[53] Qu X, Peng Z, Wang Y and Dong S 2005 *Electroanalysis* **17** 59
[54] Liu J, Rinzler A G, Dai H, Hafner J H, Kelley Bradley R, Boul P J, Lu A, Iverson T, Shelimov K, Huffman C B, Rodriguez-Macias F, Shon Y-S, Randall Lee T, Colbert D T and Smalley R E 1998 *Science* **208** 1253
[55] Louie G V and Brayer G D 1990 *J. Mol. Biol.* **214** 527
[56] Andolfi L, Bizzarri A R and Cannistraro S 2006 *Thin Solid Films* **515** 212
[57] Bizzarri A R, Bonanni B, Costantini G and Cannistraro S 2003 *Chem. Phys. Chem.* **4** 1189
[58] Vesenka J, Guthold M, Tang C L, Keller D, Delain E and Bustamante C 1992 *Ultramicroscopy* **42** 1243

[59] Gwyer J D, Zhang J, Butt J N and Ulstrup J 2006 *Biophys. J.* **91** 3897
[60] Andolfi L, Cannistraro S, Canters G W, Facci P, Ficca A G, Van Amsterdam I M C and Verbeet M Ph 2002 *Arch. Biochem. Biophys.* **399** 81
[61] Losic D, Shapter J G and Gooding J J 2002 *Langmuir* **18** 5422
[62] Chi Q, Zhang J, Nielsen J U, Friis E P, Chorkendorff I, Canters G W, Andersen J E T and Ulstrup J 2000 *J. Am. Chem. Soc.* **122** 4047
[63] Davis J J, Morgan D A, Wrathmell C L and Zhao A 2004 *IEE Proc. Nanobiotechnol.* **151** 37
[64] Facci P, Alliata D and Cannistraro S 2001 *Ultramicroscopy* **89** 291
[65] Alliata D, Andolfi L and Cannistraro S 2004 *Ultramicroscopy* **101** 231
[66] Rao A M, Richter E, Bandow S, Chase B, Eklund P C, Williams K A, Fang S, Subbaswamy K R, Menon M, Thess A, Smalley R E, Dresselhaus G and Dresselhaus M S 1997 *Science* **275** 187
[67] Kurti J, Kresse G and Kuzmany H 1998 *Phys. Rev.* B **58** R8869
[68] Saito R, Takeya T, Kimura T, Dresselhaus G and Dresselhaus M S 1998 *Phys. Rev.* B **57** 4145
[69] Salemme F R 1976 *J. Mol. Biol.* **1025** 563
[70] Chen S, Shen W, Wu G, Chen D and Jiang M 2005 *Chem. Phys. Lett.* **402** 312
[71] Peng H, Alemany L B, Margrave J L and Khabashesku V N 2003 *J. Am. Chem. Soc.* **125** 15174
[72] Kurti J, Kuzmany H, Burger B, Hulman M, Winter J and Kresse G 1999 *Synth. Met.* **103** 2508
[73] Alvarez L, Righi A, Rols S, Anglaret E, Sauvajol J L, Munoz E, Maser W K, Benito A M, Martinez M T and de la Fuento G F 2001 *Phys. Rev.* B **63** 153401
[74] Rao A M, Chen J, Richter E, Schlecht U, Eklund P C, Haddon R C, Venkateswaren U D, Kwon Y K and Tomanek D 2001 *Phys. Rev. Lett.* **86** 3895
[75] Delfino I, Bizzarri A R and Cannistraro S 2005 *Biophys. Chem.* **113** 41
[76] Delfino I, Bizzarri A R and Cannistraro S 2006 *Chem. Phys.* **326** 356
[77] Lee I, Lee J W and Greenbaum E 1997 *Phys. Rev. Lett.* **79** 3294
Cui X D, Zarate X, Tomfohr J, Sankey O F, Primak A, Moore A L, Moore T A, Gust D, Harris G and Lindsay S M 2002 *Nanotechnology* **13** 5
[78] Solomon A, Cahen D, Lindsay S, Tomfohr J, Engelkes V B and Friesbie C D 2003 *Adv. Mater.* **15** 1881
[79] Andolfi L, Bizzarri A R and Cannistraro S 2006 *Appl. Phys. Lett.* **89** 183125
[80] Beebe J M, Engelkes V B, Miller L L and Friesbie C D 2002 *J. Am. Chem. Soc.* **124** 11268
[81] Palermo V, Palma M, Tomovìc Z, Watson M D, Friedlein R, Mullen K and Samorì P 2005 *Chem. Phys. Chem.* **6** 2371